RESEARCH ARTICLE

Responsibility Division for Harmonic Instability in the Multi-Paralleled Grid-Connected Inverters System Based on Impedance Analysis

CHENGBI ZENG [ID] 1, XUEFENG WU [ID] 1, HONG MIAO [ID] 1, AND HAOXIANG DUAN 2

[1]College of Electrical Engineering, Sichuan University, Chengdu 610044, China
[2]Chengdu Rail Transit Group Company Ltd., Chengdu 610044, China

Corresponding author: Haoxiang Duan (1604681549@qq.com)

ABSTRACT In the multi-paralleled grid-connected inverters system, harmonic oscillations may be deteriorated or even lead to system instability by the coupling between the inverters and the grid impedance. This paper presents a quantify method to determine which inverters contribute more to the harmonic instability so that the corresponding inverters can be removed quickly or targeted oscillation suppression measures can be taken to restore the system to stable operation. In the method, a contribution factor (CF_i) is defined which can quantitatively represent the responsibility of each inverter to system instability. The CF_i are calculated by analyzing the variation of system stability margin after different inverters are removed based on the bode diagram, therefore, according to the corresponding CF_i, which inverters have a significant impact on harmonic instability can be determined under different grid impedances. Besides used in the parallel system with different types of inverters (PSDI), the CF_i can also be used for the parallel system with identical inverters (PSII) to determine the number of inverters that need to be removed to restore the system to stable operation. The reasonableness and effectiveness of the proposed method are verified by simulation results.

INDEX TERMS Grid-connected inverters, responsibility division, stability analysis, weak grid, harmonic oscillations.

I. INTRODUCTION

With the increasing penetration of renewable energy generation connected to the grid, the stability issues of the multi-paralleled grid-connected inverters system have become increasingly prominent [1], [2]. Parallel inverters, different types of inverters in particular, are coupled to each other through grid impedance, and the coupling effect may cause harmonic oscillations or even lead to system instability [3], [4]. Furthermore, under the condition of weak grid, the interaction effect between grid impedance and the output impedance of inverters will further aggravates the system instability problem [5], [6].

Most research works on harmonic instability in the multi-paralleled grid-connected inverters system mainly focuses on predicting system stability and exploring various measures to improve system stability, such as deriving stability criteria based on impedance analysis [7], [8], [9], or redesigning the control strategy of each inverter to achieve oscillation suppression [10], [11], [12], [13], [14], [15]. However, the overall parallel system may still experience resonance or even instability even if all inverters individually meet the stability criteria [2], [6], [11]. In this case, compared to taking corresponding measures for each inverter, identifying the responsibility of each inverter for harmonic instability to carry out targeted stability measures, namely responsibility division, is a relatively simple and effective method to restore the system stability. In practical industrial applications, the identified main inverters which contribute more

The associate editor coordinating the review of this manuscript and approving it for publication was Suman Maiti [ID].

to the harmonic instability are considered the most effective position for active or passive damping activities or can be directly disconnected in the emergency event of system instability [16], [17], [18].

At present, a commonly method for responsibility division is based on the state-space model, where the responsibility of each inverter can be identified by calculating the participation factor from its state space matrix [19], [20], [21]. However, this method is not suitable for a large-scale power system that involves numerous inverters connected, as the introduction of a large number of state variables will make the state space matrix too complex. Compared with the state-space analysis, the impedance-based analysis is more widely used as a powerful tool for predicting harmonic stability [22], [23], [24], [25]. However, in the presently research based on impedance analysis, little attention was paid to the contribution of individual inverter to the system harmonic instability. In [16], the impedance modeling and resonant mode analysis are combined to locate which inverters have a significant contribution to the harmonic instability. However, this method involves performing eigenvalue decomposition on the system's multi-input multi-output transfer function matrix, which limits its suitability for carrying out corresponding action in emergency instability situation. A new method for diagnosing which particular inverter causes instability is proposed in [17] based on comparison between the root-mean-square value of harmonic voltage at the point of common coupling (PCC) and the harmonic voltage across the filters capacitors when the internal instability occurs in the overall interconnected system. However, it requires additional sensors and is only suitable for situations where the inverter experiences internal instability. A responsibility identification method based on global admittance-based stability criterion is proposed in [18] and [26], which identify the responsibility of the inverter for system instability by quantifying the distance between the real part of the equivalent output admittance and the system's instability boundary. However, the method requires repeated calculations of the real and imaginary parts of the output admittance of each inverter in the frequency domain and also suffers the problem of large amount of calculation. In addition, these methods presented in [16], [17], [18], and [26] are analyzed in the case that grid impedance is constant. Actually, with the different penetration of renewable energy generation, the grid impedance varies and further exploration should be carried out to determine the individual inverter's contribution to system instability under this condition.

This paper presents a brief and effective responsibility division method based on the impedance analysis for determining the contribution of individual inverter to harmonic instability in the multi-paralleled grid-connected inverters system. In the method, a contribution factor (CF_i) is defined to quantify the responsibility of each inverter to system instability, which is calculated based on the variation of system stability margin after the corresponding inverter is taken out of operation. Compared with the previous research work, the main contributions of this paper are as follows:

1) The proposed method relies entirely on the frequency characteristics of the output admittance of each inverter, which can be obtained in advance through experiments or numerical simulations, so it can be easily applied to large-scale power electronic systems which faces instability problem.

2) The CF_i directly reflects the effect of the corresponding inverter on the system stability margin. A larger CF_i means a larger contribution to the harmonic instability, therefore, the responsibility of different inverters for system instability is simply and directly quantitatively represented.

3) The effects of variable grid impedance on the responsibility of each inverter to system instability are analyzed, which is typical meaningful for the system with the different penetration of renewable energy generation.

The rest of the paper is organized as follows. In Section II, the modeling of the parallel system with different types of inverters (PSDI) are described and its stability conditions are derived. In Section III, the impact of different types of inverters exiting operation on system stability are analyzed. In Section IV, the responsibility division method is presented, where the CF_i is calculated to identify the inverter that contributes the most to harmonic instability and it can be used to determine which inverters should be removed to restore system stability in the PSDI. In addition, for the parallel system with identical inverters (PSII), the application of the CF_i to determine the number of inverters that need to be removed to restore the system to stable operation is presented. In Section V, the application of the proposed method is further illustrated by case studies under different grid impedance conditions. In Section VI, the feasibility of the proposed method is verified by building a simulation model. The conclusions are drawn in Section VII.

II. THE MODELING AND STABILITY ANALYSIS FOR THE PSDI
A. MATHEMATICAL MODEL OF THE PSDI
The topology of the investigated PSDI is shown in Fig.1, where multiple inverters of different types are connected to the PCC through an output filter, and V_g represents e grid voltage. V_{CN}, i_N, L_{1N}, C_N and L_{2N} are the voltage on the filter capacitor, the grid-connected current, the inverter-side inductance, the filter capacitor and the grid-side inductance for the Nth inverter in the system, respectively. Z_g and V_{in} are the grid impedance and the inverter DC-side input voltage, respectively. In order to take into account the general situation, it is assumed that the parameters and control structure of each inverter are different.

As shown in Fig.1, the voltage of the Nth inverter at the PCC can be expressed as:

$$V_{PCC} = Z_g(s) \sum_{1,j \neq N}^{n} i_j(s) + V_g(s) \tag{1}$$
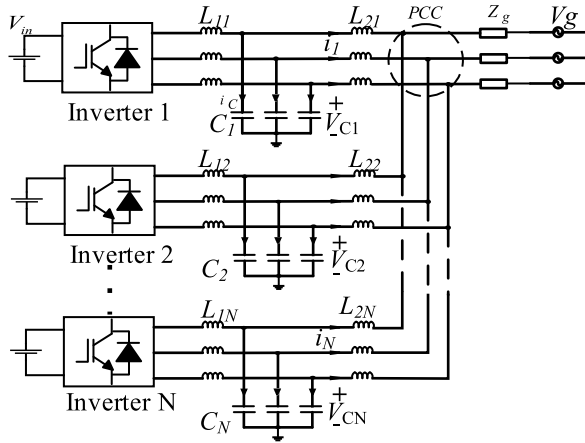
FIGURE 1. Structure diagram of the multi-paralleled grid-connected inverters system.

The grid-connected current of the Nth inverter can be expressed as [27]:

$$i_N(s) = G_N(s)i_N^*(s) - Y_N(s)V_{PCC} \quad (2)$$

where $G_N(s)$ is the transfer function between the grid-connected current $i_N(s)$ of the inverter and its command value $i_N^*(s)$. $Y_N(s)$ is the transfer function between the voltage of the PCC and the grid-connected current of the inverter, which is defined as the output admittance of the inverter [28]. Substituting (1) into (2), the grid-connected current can be rewritten as:

$$i_N(s) = G_N(s)i_N^*(s) - Y_N(s)(V_g(s) + Z_g(s)\sum_{j=1,j\neq N}^{n} i_j(s)) \quad (3)$$

It can be seen from (3) that due to the grid impedance $Z_g(s)$, the output current of each inverter are influenced by the output current of other inverters in the PSDI, namely inverters are mutual coupling.

The grid-connected current can be rewritten as:

$$i_N(s) = i_{0N}(s) - Y_N(s)Z_g(s)\sum_{j=1,j\neq N}^{n} i_j(s) \quad (4)$$

where $i_{0N}(s)$ presents the output current of the Nth inverter when it is connected to the ideal grid alone.

The PSDI is actually a typical MIMO system, the relationship between i_{0N} and i_N of each inverter can be written by using the transfer function matrix as shown in (5), where the outputs are the grid-connected currents for parallel operation and the inputs are the grid-connected currents when connected to the ideal grid:

$$\begin{bmatrix} i_1 \\ i_2 \\ \cdots \\ i_n \end{bmatrix} = \begin{bmatrix} G_{11}(s) & G_{12}(s) & \cdots & G_{1n}(s) \\ G_{21}(s) & G_{22}(s) & \cdots & G_{2n}(s) \\ \cdots & \cdots & \cdots & \cdots \\ G_{n1}(s) & G_{n2}(s) & \cdots & G_{nn}(s) \end{bmatrix} \begin{bmatrix} i_{01} \\ i_{02} \\ \cdots \\ i_{0n} \end{bmatrix} \quad (5)$$

Where

$$\begin{cases} G_{ij}(s) = 1 - \dfrac{Y_i(s)}{\frac{1}{Z_g(s)}+\sum\limits_{i=1}^{n} Y_i(s)}(i = j) \\ G_{ij}(s) = -\dfrac{Y_i(s)}{\frac{1}{Z_g(s)}+\sum\limits_{i=1}^{n} Y_i(s)}(i \neq j) \end{cases} \quad (6)$$

The dynamic transfer relationship between the input and the output of the PSDI can be further represented by Fig.2.
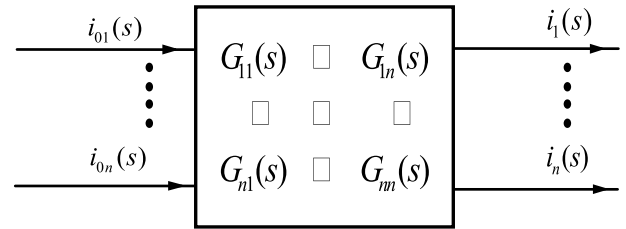

FIGURE 2. The mathematical model of the PSDI.

It can be seen that the necessary condition for the stability of the PSDI is the stability of each i_{0N}, namely each inverter is stable when connected to the ideal grid with assumption of $Z_g(s)=0$.

B. STABILITY ANALYSIS

Substituting (6) into (5), the grid-connected current can be rewritten as:

$$i_N(s) = i_{0N}(s) - \frac{Y_N(s)}{\frac{1}{Z_g(s)}+\sum\limits_{i=1}^{n} Y_i(s)}\sum_{j=1}^{n} i_{0j}(s) \quad (7)$$

The expression for the total grid-connected current is as follows:

$$i(s) = \sum_{N=1}^{n} i_N(s) = \frac{Y_g(s)}{Y_g(s)+\sum\limits_{i=1}^{n} Y_i(s)}\sum_{j=1}^{n} i_{0j}(s) \quad (8)$$

where $Y_g(s) = 1/Z_g(s)$ is the grid admittance.

It can be seen from (8) that in the PSDI, due to the appearance of grid admittance $Y_g(s)$ and the difference in output admittance $Y(s)$ of inverters, the output currents of inverters are redistributed in the network.

Combined with the impedance-based stability criterion for a single grid-connected inverter in [23], the necessary and sufficient conditions for the stability of the total grid-connected current can be concluded as follows:

1) Each inverter can operate independently and stably under ideal grid conditions;

2) The sum of the output admittance of each inverter and the grid admittance $Y_g(s) + \sum_{i=1}^{n} Y_i(s)$ does not have a right half-plane zero point.

III. ANALYSIS OF THE CONTRIBUTION OF DIFFERENT INVERTERS TO SYSTEM STABILITY

A. ANALYSIS OF SYSTEM INSTABILITY

As stated in section II, the first stability condition can be easily satisfied with properly design of the current regulator [29]. Moreover, the second condition implies that the amplitude-frequency characteristic curves of $Y_g(s)$ and $\sum_{i=1}^{n} Y_i(s)$ have no intersection, or phase margin(PM) is greater than 0 at the intersection frequency [30], i.e.:

$$PM = 180^\circ - \left[\angle \sum_{i=1}^{n} Y_i(f_r) - \angle Y_g(f_r) \right] > 0^\circ \quad (9)$$

Since the resistive component in the grid impedance can provide damping and thus benefit to the stable operation of the system, the analysis in this paper considers the worst case that the grid impedance is purely inductive and $Y_g(s) = 1/sL_g$. The phase of $Y_g(s)$ is always equal to -90°, therefore, the phase of the $\sum_{i=1}^{n} Y_i(s)$ at the intersection frequency should be less than 90° to satisfy the second condition.

On the premise that the first condition is satisfied, $Y_g(s) + \sum_{i=1}^{n} Y_i(s)$ does not contain the right half-plane pole, then the second condition can also be translated into that the Nyquist curve of $Y_g(s) + \sum_{i=1}^{n} Y_i(s)$ does not enclose the origin, which is reflected in the Bode diagram as the phase-frequency characteristic of $Y_g(s) + \sum_{i=1}^{n} Y_i(s)$ does not cross the 180° line. If the crossing occurs, the crossing frequency is the intersection frequency.

Taking a PSDI system which contains four different type of inverters for example, and its vector diagram of the output admittance at intersection frequency can be presented in Fig.3, where Y_1, Y_2, Y_3, Y_4 are the output admittance of the four inverters, respectively. As it can be observed, the phase of $Y_1 + Y_2 + Y_3 + Y_4$ is greater than 90°, and removing Y_3 or Y_4 may make the phase of the sum of the remaining inverters output admittance smaller, which facilitates the stable operation of the system. After removing Y_3, the phase θ' of $Y_1 + Y_2 + Y_4$ is still greater than 90°. By comparison, the phase θ of $Y_1 + Y_2 + Y_3$ is less than 90° after removing Y_4. It is indicated that Y_1, Y_2 and Y_3 parallel operation is stable while Y_1, Y_2 and Y_4 parallel operation is unstable.
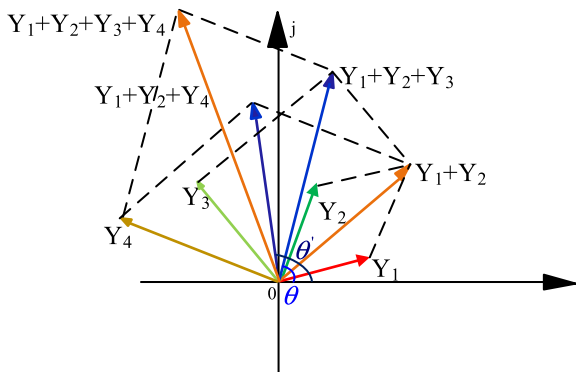
As shown in Fig.3, the existence of inverters with the phase of the output admittance greater than 90° at the intersection frequency is a necessary condition for the instability of the system, however, exiting the operation of different inverters has different impacts on system stability. Therefore, it is crucial to determine the impact of different types of inverters exiting operation on system stability.

B. THE IMPACT OF DIFFERENT TYPES OF INVERTERS EXITING OPERATION ON SYSTEM STABILITY

Taking the typical dual loop control structure of capacitor current feedback active damping combined with grid side current feedback as an example [27], the amplitude-frequency characteristics of the grid admittance, and the sum of output admittance of different numbers of inverters are shown in Fig.4, where $\sum_{i=1,i\neq j}^{n} Y_i(s)$ represents the sum of the output admittance of the remaining inverters after the jth inverter is removed from the system. ω_0 is the initial intersection frequency, and ω_1 is the new intersection frequency after the jth inverter is removed.
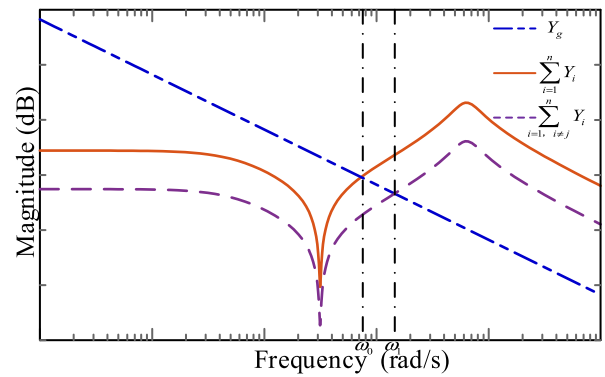

FIGURE 4. Amplitude-frequency characteristics of the grid admittance and the sum of output admittance of different numbers of inverters.

From Fig.4, the relationship between the ω_0 and ω_1 can be expressed as:

$$\frac{20\lg Abs[\sum_{i=1,i\neq j}^{n} Y_i(j\omega_1)] - 20\lg Abs[(\sum_{i=1}^{n} Y_i(j\omega_0)]}{\lg \omega_1 - \lg \omega_0} = -20 \quad (10)$$

Equation (10) can be rewritten as:

$$20\lg \omega_0 Abs[\sum_{i=1}^{n} Y_i(j\omega_0)] = 20\lg \omega_1 Abs[\sum_{i=1,i\neq j}^{n} Y_i(j\omega_1)] \quad (11)$$

when the jth inverter is taken out of operation, the new intersection frequency of the system is determined by (11).

To simplify the analysis, Fig.5 shows the amplitude-frequency characteristics of the corresponding equivalent output admittance of the system after removing different numbers of inverters, where k represents the number of inverters removed and $s\sum_{i=1}^{n} Y_i(s)$ is considered as the equivalent
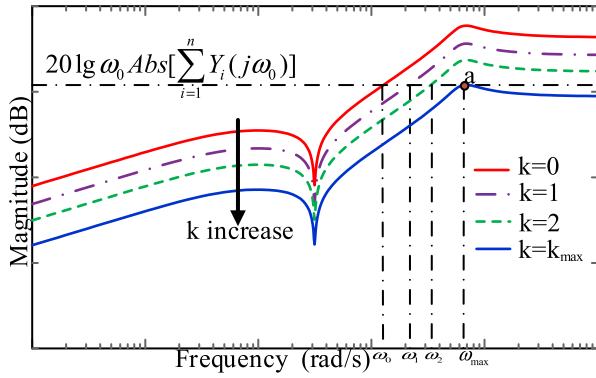

FIGURE 3. Vector diagram of the output admittance of multiple inverters.

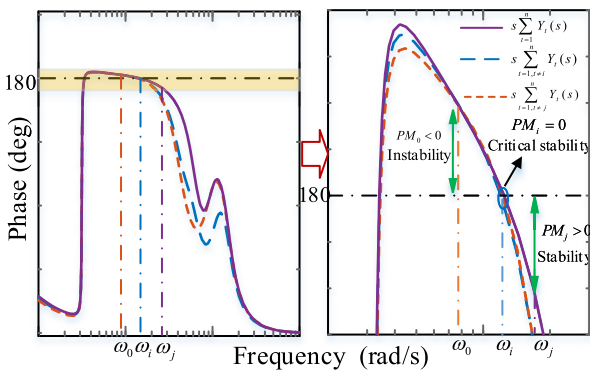**FIGURE 5.** Amplitude-frequency characteristics of equivalent output admittance of the system.

FIGURE 6. The corresponding system phase margin after removing different inverters.

output conductance of the system in the initial state k=0. According to (11), the new intersection frequency ω_k can always be found at each frequency point corresponding to the initial amplitude $20 \lg \omega_0 Abs[\sum_{i=1}^{n} Y_i(j\omega_0)]$.

When the amplitude-frequency characteristics curve of the equivalent output admittance drops to its maximum value equal to the initial amplitude, as shown at point (a) in Fig.5, i.e.:

$$\max[Abs(s \sum_{j=1}^{n-k_{max}} Y_j(s))] = 20 \lg \omega_0 Abs[\sum_{i=1}^{n} Y_i(j\omega_0)] \quad (12)$$

the corresponding k_{max} is the maximum number of inverters that need to be removed to restore system stability.

The stability state of the system after removing different inverters depends on the phase of the sum of the output admittances of the remaining inverters at the new intersection frequency, which can be expressed as:

$$PM = 90° - \angle \sum_{i=1,i\neq j}^{n} Y_i(s) = 180° - \angle \sum_{i=1,i\neq j}^{n} sY_i(s) \quad (13)$$

Fig.6 shows the corresponding system phase margin after removing different inverters, where PM_0, PM_i and PM_j are the phase margin at initial intersection frequency ω_0, the corresponding intersection frequency ω_i after removing the

ith inverter and the corresponding intersection frequency ω_j after removing the jth inverter, respectively. It is evident that removing different types of inverters from the system results in different stability margins, which correspond to different system operating states.

The change in the phase margin of the system caused by the ith inverter can be expressed as:

$$\Delta_i = PM_i - PM_0 \quad (14)$$

As shown in Fig.6, since $PM_0 < 0$, the system will oscillates at the initial intersection frequency ω_0. When the phase margin of the system is changed, the relationship between the amount of change and the operating state of the system can be derived as:

$$\begin{cases} \Delta_i < |PM_0| & \text{Instability} \\ \Delta_i = |PM_0| & \text{Critical stability} \\ \Delta_i > |PM_0| & \text{Stability} \end{cases} \quad (15)$$

Equation (15) shows that the inverter corresponding to $\Delta_i > |PM_0|$ can be identified as the unstable factor in the system. The magnitude of Δ_i represents the degree of change in the operating states, so a larger Δ_i indicates that this inverter has a greater impact on system stability.

Substituting (13) into (14), the change in the phase margin of the system can be rewritten as:

$$\Delta_i = \angle \sum_{t=1}^{n} j\omega_0 Y_t(j\omega_0) - \angle \sum_{t=1,t\neq i}^{n} j\omega_i Y_t(j\omega_i) \quad (16)$$

The amplitude relationship of the system equivalent output admittances at different intersection frequencies can be derived as follows:

$$\omega_0 Abs[\sum_{t=1}^{n} Y_t(j\omega_0)] = \omega_i Abs[\sum_{t=1,t\neq i}^{n} Y_t(j\omega_i)] = \frac{1}{L_g} \quad (17)$$

Fig.7 shows the relationship between the amplitude and phase angle of the $s \sum_{t=1}^{n} Y_t(s)$, $s \sum_{t=1,t\neq i}^{n} Y_t(s)$, $s \sum_{t=1,t\neq j}^{n} Y_t(s)$ in the polar coordinate system. According to (17), the larger the grid inductance, the smaller the amplitude of the system equivalent output admittances at the
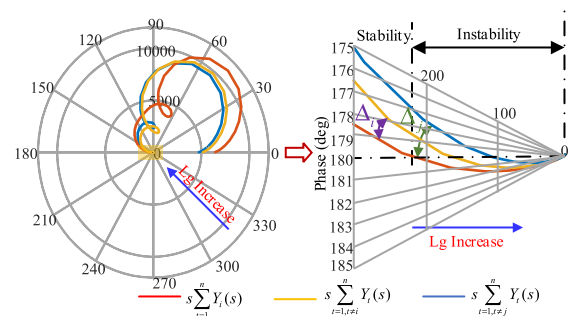

FIGURE 7. The relationship between the amplitude and phase angle of the $s \sum_{t=1}^{n} Y_t(s)$, $s \sum_{t=1,t\neq i}^{n} Y_t(s)$ and $s \sum_{t=1,t\neq j}^{n} Y_t(s)$.

intersection frequency. As shown in Fig.7, as the grid inductance increases, the stability margin of the system gradually decreases. However, the Δ_j is always greater than the Δ_i, indicating that the jth inverter always has a greater impact on the system stability. This is due to the fact that the output admittance amplitude of the jth inverter is always greater than the output admittance amplitude of the ith inverter at the same phase angle. It can be concluded that the variable grid impedance does not change the responsibility of each inverter, and the inverters with a larger output admittance amplitude always contribute more to system instability.

IV. PROPOSED RESPONSIBILITY DIVISION METHOD
A. RESPONSIBILITY DIVISION FOR THE PSDI

In this paper, in order to quantitatively compare and analyze the impact of each individual inverter on system stability, the variations in system phase margin corresponding to each inverter are normalized and defined by a contribution factor (CF_i). This contribution factor (CF_i) can be expressed as:

$$CF_i = \frac{\Delta_i}{\sum\limits_{j=1}^{n} \Delta_j} \qquad (18)$$

The larger the CF_i, the greater the contribution of the corresponding inverter to system instability and vice versa. The contribution factor corresponding to the critical stability of the system can be expressed as:

$$CF^* = \frac{|PM_0|}{\sum\limits_{i=1}^{n} PM_i + n\,|PM_0|} \qquad (19)$$

Equation (19) shows that CF^* is influenced by the initial oscillation frequency, the output admittance of each inverter and the number of parallel inverters. If the CF_i corresponding to the ith inverter is greater than CF^*, it means that the system can be restored to stable operation by removing only the ith inverter. Conversely, if all CF_i are less than CF^*, it indicates that the system needs to remove more inverters to restore stability.

According to above analysis, the specific steps of the method of dividing responsibility proposed in this paper are summarized as follows:

1) Get the frequency response of output admittance Y_i of each inverter and grid admittance Y_g;
2) Calculate the phase frequency characteristics of $Y(s) = Y_g(s) + \sum_{i=1}^{n} Y_i(s)$. If it does not cross the 180° line, the system is stable and the process is finished. If it crosses the 180° line, the system is destabilized and record the oscillation frequency f_r;
3) Calculate the phase $\angle Y_i(f_r)$ of the output admittance of each inverter at the oscillation frequency. Then record the set S which consists of the inverters with $\angle Y_i(f_r) > 90°$, and the number of elements of S is denoted as card(S)=t;

4) Calculate the contribution factor CF_i corresponding to each inverter in the S set and the CF^* corresponding to the critical stability of the system;
5) If the maximum CF_i is greater than CF^*, it indicates that the system can be restored to stable operation by removing single inverter. If the maximum CF_i is smaller than CF^*, remove the inverters in order of CF_i from large to small until the system is stable.
6) After the system is stabilized, the inverter that is recorded to be removed from the system is the group of inverters with the most responsible for instability.

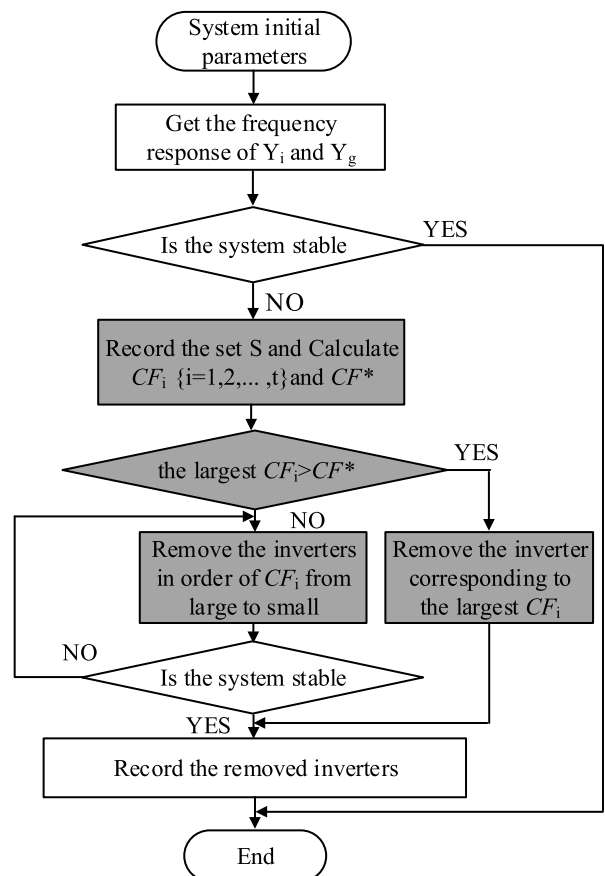The flow chart of the method is shown in Fig.8.

FIGURE 8. Flow chart of the responsibility division method.

B. APPLICATION OF THE PROPOSED METHOD IN THE PSII
The above analysis can also be used to the PSII, which contains multiple identical inverters. For the PSII, the drop in intersection frequency caused by removing each inverter from the system is equal, so the CF_i of each inverter is also the same.

Fig.9 shows the frequency characteristics of the PSII under different operating states. ω_0 is the initial oscillation frequency of the system, and $\omega_1, \omega_i, \omega_{i+1}$ are the new intersection frequency after one, i and i+1 inverters removed from the system, respectively.

TABLE 1. System parameters.

Symbol	Description	Inverter 1	Inverter 2	Inverter 3
V_{dc}	DC voltage	360 V	360 V	360 V
V_{tri}	Amplitude of triangle carrier wave	2V	2V	2V
L_1	Inverter-side inductance	2mH	1.5mH	1.2mH
L_2	Grid-side inductance	0.8mH	0.3mH	0.6mH
C	Filter capacitance	10uF	8uF	10uF
H_{il}	Capacitive current sampling coefficient	0.3	0.28	0.25
f_0	Grid frequency	50Hz	50Hz	50Hz
f_s	Sampling frequency	10kHZ	10kHZ	10kHZ
V_g	Grid voltage	220V	220V	220V
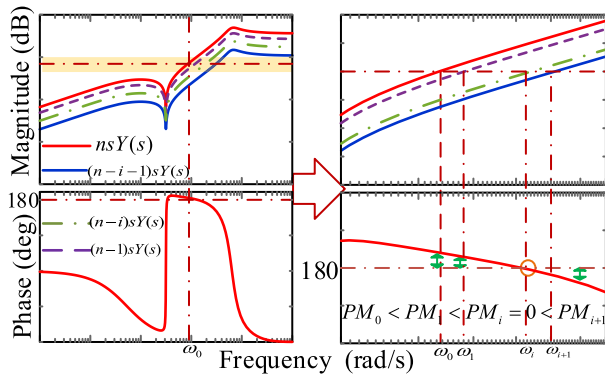
FIGURE 9. Frequency characteristics of the multiple identical inverters parallel operation system.

FIGURE 10. The phase-frequency characteristic of $Y_g(s) + \sum_{i=1}^{3} Y_i(s)$.

As shown in Fig.9, the system phase margin PM_1 corresponding to the removal of one inverter is less than 0, and the system phase margin can be greater than 0 only if a sufficient number of inverters are removed so that the intersection frequency is greater than $\omega_i (\angle sY(j\omega_i) = 180°, PM_i=0)$. Therefore, reducing the number of inverters can restore the stability of the system. The lower the oscillation frequency after instability, the more inverters need to be removed.

If the CF_i is greater than the CF^*, it means that the system can be restored to stable operation by removing single inverter. Otherwise, the number of inverters that need to be removed to restore the system to stable operation can be expressed as:

$$N = \left[CF^*/CF_i \right] + 1 \qquad (20)$$

V. CASE STUDIES UNDER DIFFERENT GRID IMPEDANCE CONDITIONS
A. APPLICATION IN THE PSDI
A case study of a PSDI under different grid impedance conditions is carried out to investigate the effectiveness of the proposed responsibility division method. The investigated PSDI system has three inverters and the parameters of the inverters are shown in Table 1. In order to achieve static error-free tracking of the grid-connection current,
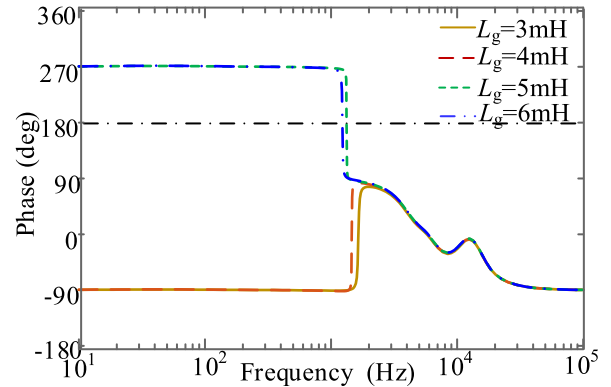
a Quasi-Proportional-Resonant (QPR) controller is used as the current controller due to its advantages of fast response speed and high robustness [31]. Its expression is shown below:

$$G_i(s) = kp + \frac{2k_r \omega_i s}{s^2 + 2\omega_i s + \omega_0^2} \qquad (21)$$

where k_p is the proportional coefficient, k_r is the resonance coefficient, ω_i is the resonance bandwidth coefficient, and ω_0 is fundamental angular frequency.

Fig.10 shows the phase-frequency characteristic of $Y_g(s) + \sum_{i=1}^{3} Y_i(s)$ with different grid impedance, where Y_1, Y_2 and Y_3 are the output admittance of inverter 1, inverter 2 and inverter 3, respectively. Evidently, when the grid inductance is greater than 5mH, the system will lose stability.

Fig.11 shows the frequency characteristics of the system under different operating states when $Lg=5mH$. ω_0 is the initial oscillation frequency of the system, and ω_1, ω_2, ω_3 are the new intersection frequency after inverter 1, 2, 3 removed from the system, respectively. It can be seen that the phase of the output admittance of all inverters are greater than 90° at the initial oscillation frequency, so every CF_i corresponding to each inverter need to be calculated. Besides, after removing the corresponding inverter, the relationship between the magnitude of the phase margin is $PM_3 > PM_1 > 0 > PM_2$, indicating that inverter 3 is the most responsible for system
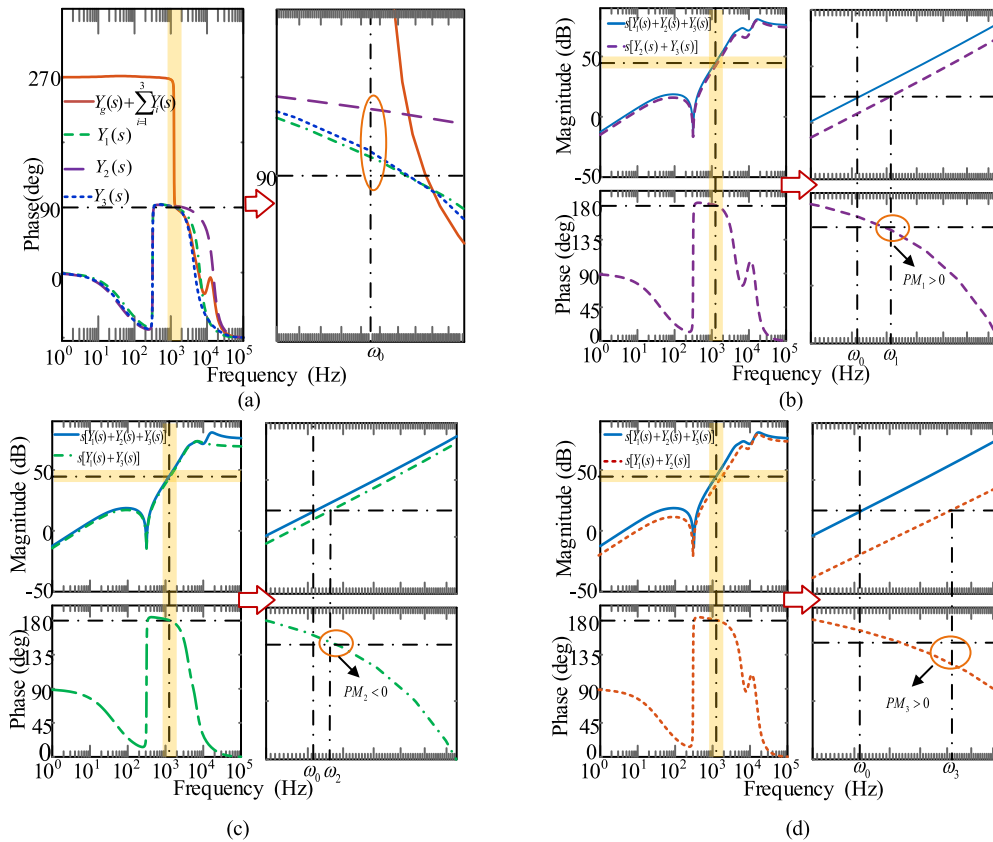
FIGURE 11. Frequency characteristics of the system under different operating states when Lg=5mH. (a) Three inverters operate in parallel;(b) Remove Inverter 1; (c) Remove Inverter 2; (d) Remove Inverter 3.

TABLE 2. The contribution factors of each inverter under different grid inductances.

Cases	CF_1	CF_2	CF_3	CF^*
L_g=5mH	0.23	0.20	0.57	0.22
L_g=7mH	0.21	0.16	0.63	0.46
L_g=10mH	0.14	0.20	0.66	0.82
L_g=12mH	0.16	0.23	0.61	0.73
L_g=15mH	0.11	0.21	0.68	1.27
L_g=20mH	0.11	0.22	0.67	1.52

TABLE 3. The contribution factors of the corresponding inverter under different grid inductances.

Cases	CF_{1+3}	CF_{2+3}	CF^*
L_g=10mH	0.35	0.65	0.34
L_g=12mH	0.36	0.64	0.42
L_g=15mH	0.39	0.61	0.53
L_g=20mH	0.41	0.59	0.65

instability while inverter 1 and inverter 2 are with less responsibility instability.

The contribution factors (CF_i) of each inverter under different grid inductances are shown in Table 2. It can be seen that inverter 3 contributes the most to system instability since it always has the largest CF_i, while the system can be restored to stability after removing inverter 3 since $CF_3 > CF^*$ under the condition of L_g=5mH and L_g=7mH. On the contrast, the system will remain unstable if only inverter 3 is removed since $CF_3 < CF^*$ under the condition of $L_g \geq 10mH$.

When the grid inductance is greater than 10mH, it is necessary to take measures on more inverters to restore system stability. After removing the inverter 3, the contribution

factors of the remaining inverters under different grid inductances are calculated as shown in Table 3, where the CF_{i+j} represents the corresponding contribution factor after removing inverter i and inverter j. It is evident that the system can be restored to stable operation by removing inverter 3 and inverter 2 due to $CF_{2+3} > CF^*$ under the condition of L_g=10mH, L_g=12mH and L_g=15mH. However, when L_g=20mH, since $CF_{2+3} < CF^*$, the system will remain unstable even if inverters 2 and 3 are removed at the same time.

B. APPLICATION IN THE PSII

The proposed method is also applied to a PSII with three inverters, assuming that all the inverters are the type of inverter 1 in Table 1. Table 4 shows the number of inverters
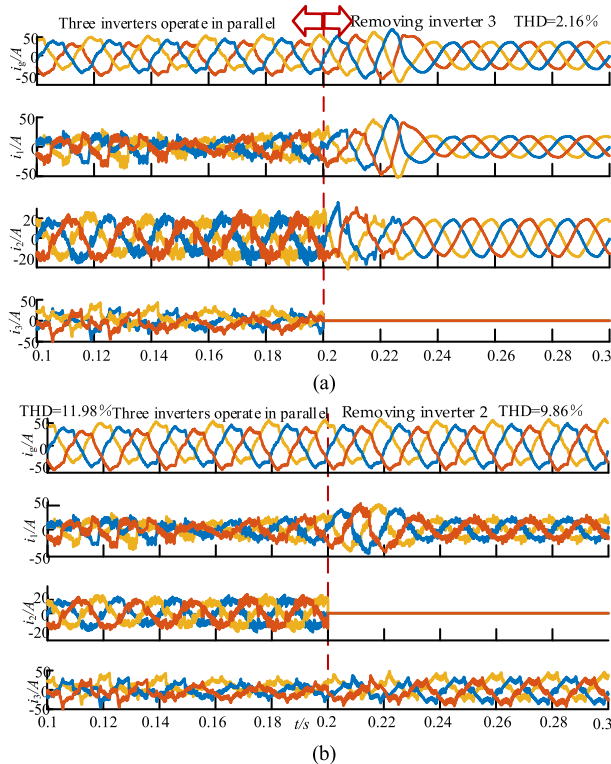
TABLE 4. The number of inverter 1 that need to be removed under different grid inductances.

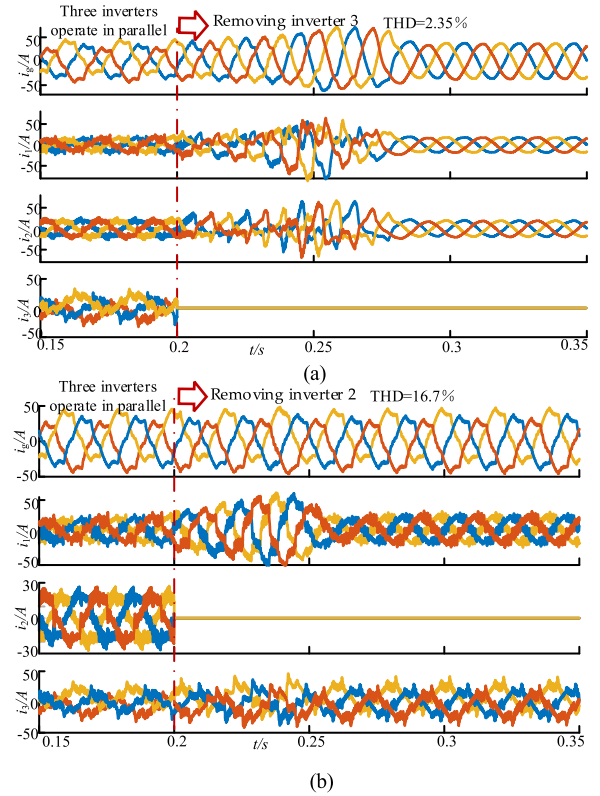| Cases	CF_1	CF^*	N
L_g=5mH	—	—	0
L_g=7mH	0.33	0.30	1
L_g=10mH	0.33	0.58	2
L_g=12mH	0.33	0.62	2
L_g=15mH	0.33	0.65	2
L_g=20mH	0.33	1.14	3
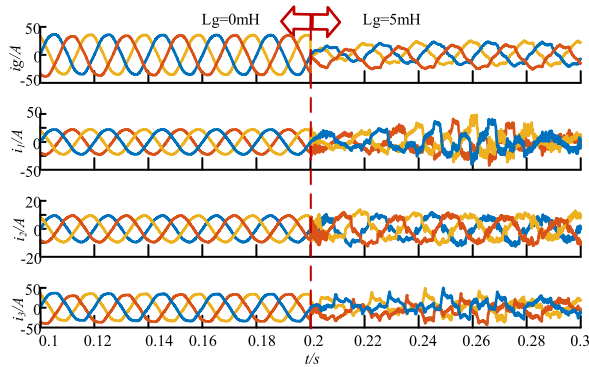
FIGURE 12. Simulation results of the PSDI under different grid inductances.

FIGURE 13. Simulation results of the PSDI when L_g=5mH. (a) Remove Inverter 3 when t=0.2s;(b) Remove Inverter 2 when t=0.2s.
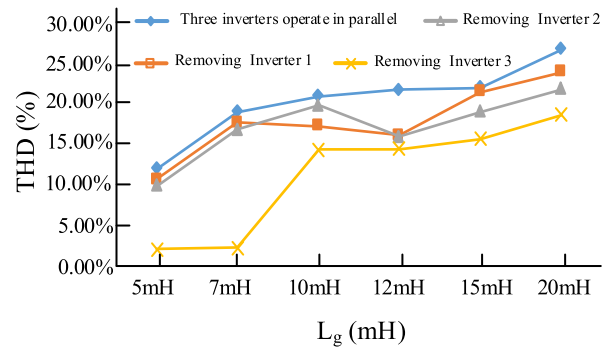

FIGURE 14. Simulation results of the PSDI when Lg=7mH. (a) Remove Inverter 3 when t=0.2s;(b) Remove Inverter 2 when t=0.2s.


FIGURE 15. The THD of the grid-connected current under different grid inductances.

to 5mH, the system can operate stably since the phase of the output admittance of inverter is less than 90° at the intersection frequency. The larger the grid inductance, the more inverters need to be removed. In the case of L_g=20mH, the system will remain unstable even if only one inverter 1 is connected to the grid.

VI. SIMULATION VERIFICATION
A. SIMULATION VERIFICATION FOR THE PSDI UNDER DIFFERENT GRID IMPEDANCES

Fig.12 shows the simulation waveforms of the PSDI under different grid inductances, where i_1, i_2, i_3 and i_g are the output current of the inverter 1, 2, 3 and the total
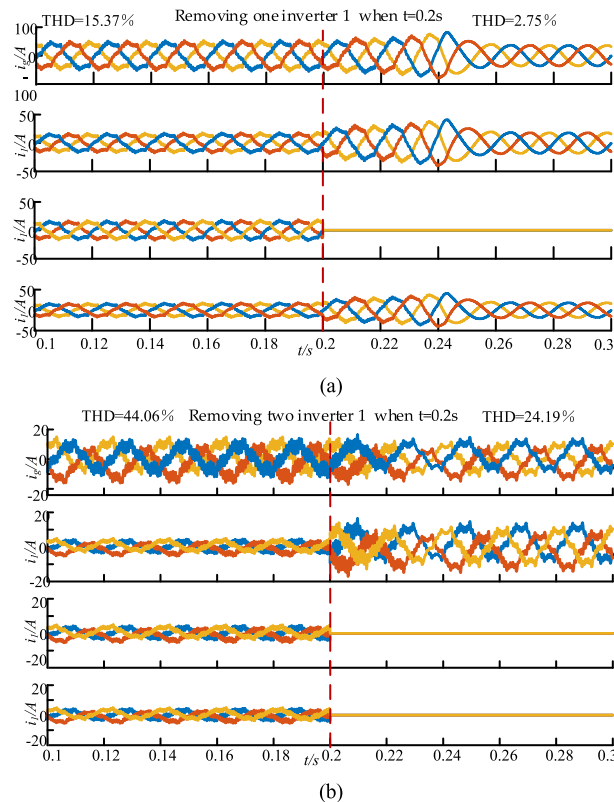
that need to be removed to restore system stability under different grid inductances. When the grid inductance is equal
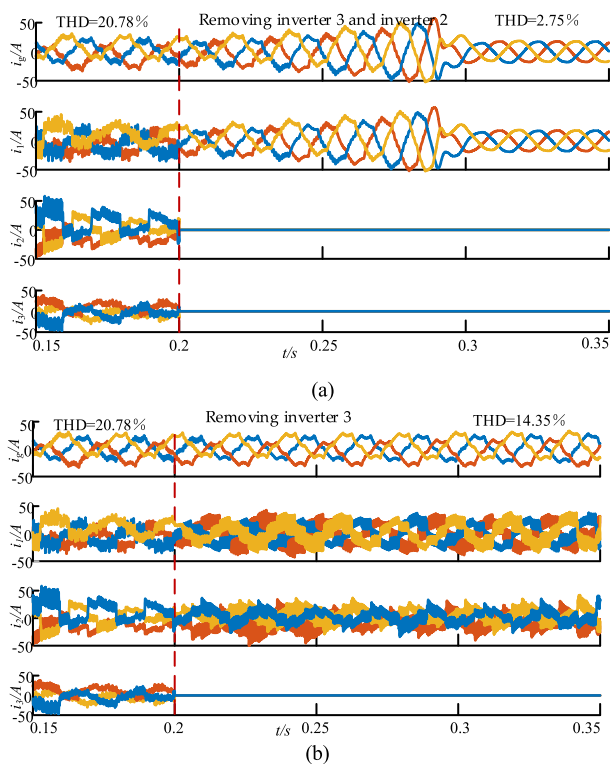
FIGURE 16. Simulation results of the PSDI when Lg=10mH. (a) Remove Inverter 3 and Inverter 2 when t=0.2s;(b) Remove Inverter 3 when t=0.2s.

FIGURE 17. Simulation results of the PSII under different grid impedances. (a) Remove one inverter 1 under the condition of Lg=7mH;(b) Remove two inverter under the condition of Lg=20mH.

grid-connection current, respectively. Although each inverter is capable of operating stably under ideal grid conditions (L_g=0mH), the parallel system still experiences oscillations when the grid inductance step up to 5mH at t=0.2s. The simulation results validate the theoretical analysis mentioned earlier.

When L_g=5mH, the simulation waveforms of the PSDI are shown in Fig.13. It is clear that the current oscillations will be damped after disconnecting inverter 3 and the total harmonic distortions (THD) of the i_g will decrease to 2.16% since inverter 3 has the largest CF_i ($CF_3 = 0.57 > CF$'=0.22). By contrast, since inverter 2 has a small CF_i and $CF_2 < CF$', the current oscillations will remain in the PSDI even after disconnecting inverter 2.

Fig.14 shows the simulation waveforms of the PSDI under the condition of L_g=7mH. In this case, the inverter 3 is still the main unstable factor of the multi-paralleled grid-connected inverters system. The system can be restored to stability by disconnecting the inverter 3. In contrast, the system is still unstable when the operation of inverter 2 is disabled.

Fig.15 illustrates the THD analysis of the grid-connected current when different inverters are removed from the system under varying grid inductances. Regardless of the specific grid impedance, it is evident that the removal of inverter 3 consistently results in the most significant reduction in THD of the grid-connected current. It indicates that inverter

3 is always the main unstable factor under different grid inductances.

Under the condition of L_g=10mH, the simulation waveforms of i_1, i_2, i_3 and i_g are shown in Fig.16. It can be seen that the current oscillations of the system will be damped after removing inverter 3 and inverter 2, and the THD of the i_g will decrease to 2.75% since CF_{2+3}=0.65 > CF^*=0.34. However, if only inverter 3 is removed, the current oscillations will remain in the PSDI since $CF_3 < CF^*$ at this time.

B. SIMULATION VERIFICATION FOR THE PSII

Fig.17 shows the simulation waveforms of the PSII with three inverter 1 under the condition of L_g=7mH and L_g=20mH. When L_g=7mH, it is clear that the system can be restored to stability by removing one inverter. In the case of L_g=20mH, the current oscillations will remain in the PSII even after disconnecting two inverters. It confirms the analysis presented in Table 4.

VII. CONCLUSION

This paper presents a method to quantify which inverters contribute more to the harmonic instability in the multi-paralleled grid-connected inverters system. The method calculates the contribution factor (CF_i) by analyzing the variation of the system stability margin after exiting the operation of different types of inverters, which can be used to identify the

main sources of harmonic instability in the system. For the PSDI, the analysis of the proposed method shows that a specific inverter always contributes the most to the instability of the system under different grid impedances. However, it does not mean that the inverter is the only source of harmonic instability in the system. For the PSII, the proposed method can be used to determine the number of inverters that need to be removed to restore the system to stable operation. The simulation results confirm that the change in grid impedance has a significant impact on the stability of the system. The larger the grid impedance, the more sources of harmonic instability in the system. The proposed method can simply and directly determine the responsibility of each inverter for harmonic instability to ensure that targeted measures can be taken quickly to restore system stability.

In future work, it is worth considering how to implement optimal design approach to maintain system stability based on the contribution of each inverter to system stability.

REFERENCES

[1] M. Lu, X. Wang, F. Blaabjerg, and P. C. Loh, "An analysis method for harmonic resonance and stability of multi-paralleled LCL-filtered inverters," in *Proc. IEEE 6th Int. Symp. Power Electron. Distrib. Gener. Syst. (PEDG)*, Aachen, Germany, Jun. 2015, pp. 1–6.

[2] C. Zheng, Q. Li, L. Zhou, B. Li, and M. Mao, "The interaction stability analysis of a multi-inverter system containing different types of inverters," *Energies*, vol. 11, no. 9, p. 2244, Aug. 2018, doi: 10.3390/EN11092244.

[3] C. Yu, X. Zhang, F. Liu, F. Li, H. Xu, R. Cao, and H. Ni, "Modeling and resonance analysis of multiparallel inverters system under asynchronous carriers conditions," *IEEE Trans. Power Electron.*, vol. 32, no. 4, pp. 3192–3205, Apr. 2017.

[4] M. Lu, X. Wang, P. C. Loh, and F. Blaabjerg, "Resonance interaction of multiparallel grid-connected inverters with LCL filter," *IEEE Trans. Power Electron.*, vol. 32, no. 2, pp. 894–899, Feb. 2017.

[5] J. He, P. Liu, and S. Duan, "Stability analysis of multi-paralleled grid-connected inverters with different controllers in weak grid condition," in *Proc. 46th Annu. Conf. IEEE Ind. Electron. Soc. (IECON)*, Jul. 2020, pp. 2350–2355.

[6] J. L. Agorreta, M. Borrega, J. López, and L. Marroyo, "Modeling and control of N-paralleled grid-connected inverters with LCL filter coupled due to grid impedance in PV plants," *IEEE Trans. Power Electron.*, vol. 26, no. 3, pp. 770–785, Mar. 2011.

[7] Q. Ye, R. Mo, Y. Shi, and H. Li, "A unified impedance-based stability criterion (UIBSC) for paralleled grid-tied inverters using global minor loop gain (GMLG)," in *Proc. IEEE Energy Convers. Congr. Expo. (ECCE)*, Jul. 2015, pp. 5816–5821.

[8] W. Cao, S. Wang, H. Kang, K. Liu, Q. Wang, and J. Zhao, "Inherent interaction analysis for harmonic oscillations in the multi-paralleled grid-connected inverter system using a sum type criterion: Global admittance (GA)," *IEEE Access*, vol. 8, pp. 8275–8285, 2020.

[9] X. Li and H. Lin, "Stability analysis of grid-connected converters with different implementations of adaptive PR controllers under weak grid conditions," *Energies*, vol. 11, no. 8, p. 2004, Aug. 2018, doi: 10.3390/EN11082004.

[10] C. Zeng, H. Wang, S. Li, and H. Miao, "Grid-voltage-feedback active damping with lead compensation for LCL-type inverter connected to weak grid," *IEEE Access*, vol. 9, pp. 106813–106823, 2021.

[11] J. He, Y. W. Li, D. Bosnjak, and B. Harris, "Investigation and active damping of multiple resonances in a parallel-inverter-based microgrid," *IEEE Trans. Power Electron.*, vol. 28, no. 1, pp. 234–246, Jan. 2013.

[12] Y. Han, "Modeling and stability analysis of *LCL*-type grid-connected inverters: A comprehensive overview," *IEEE Access*, vol. 7, pp. 114975–115001, 2019.

[13] C. Zeng, S. Li, H. Wang, and H. Miao, "A fractional phase compensation scheme of PRMRC for LCL inverter connected to weak grid," *IEEE Access*, vol. 9, pp. 167027–167038, 2021.

[14] X. Wang, F. Blaabjerg, and P. C. Loh, "Virtual RC damping of LCL-filtered voltage source converters with extended selective harmonic compensation," *IEEE Trans. Power Electron.*, vol. 30, no. 9, pp. 4726–4737, Sep. 2015.

[15] S. Yang, Q. Lei, F. Z. Peng, and Z. Qian, "A robust control scheme for grid-connected voltage-source inverters," *IEEE Trans. Ind. Electron.*, vol. 58, no. 1, pp. 202–212, Jan. 2011.

[16] E. Ebrahimzadeh, F. Blaabjerg, X. Wang, and C. L. Bak, "Bus participation factor analysis for harmonic instability in power electronics based power systems," *IEEE Trans. Power Electron.*, vol. 33, no. 12, pp. 10341–10351, Dec. 2018.

[17] W. Wu, Z. Zhao, E. Koutroulis, H. S. Chung, and F. Blaabjerg, "Autoidentification method of the 'trouble maker(s)' for internal instability in multiparalleled inverters system," *IEEE Trans. Ind. Electron.*, vol. 69, no. 1, pp. 18–28, Jan. 2022.

[18] S. Wang, "Responsibility identification for harmonic instability in grid-connected inverter-based power system with multi-point of common coupling," in *Proc. 45th Annu. Conf. IEEE Ind. Electron. Soc. (IECON)*, vol. 1, Oct. 2019, pp. 1967–1972.

[19] Y. Wang, X. Wang, F. Blaabjerg, and Z. Chen, "Harmonic instability assessment using state-space modeling and participation analysis in inverter-fed power systems," *IEEE Trans. Ind. Electron.*, vol. 64, no. 1, pp. 806–816, Jan. 2017.

[20] L. P. Kunjumuhammed, B. C. Pal, C. Oates, and K. J. Dyke, "Electrical oscillations in wind farm systems: Analysis and insight based on detailed modeling," *IEEE Trans. Sustain. Energy*, vol. 7, no. 1, pp. 51–62, Jan. 2016.

[21] Y. Wang, X. Wang, Z. Chen, and F. Blaabjerg, "Small-signal stability analysis of inverter-fed power systems using component connection method," *IEEE Trans. Smart Grid*, vol. 9, no. 5, pp. 5301–5310, Sep. 2018.

[22] X. Feng, J. Liu, and F. C. Lee, "Impedance specifications for stable DC distributed power systems," *IEEE Trans. Power Electron.*, vol. 17, no. 2, pp. 157–162, Mar. 2002.

[23] J. Sun, "Impedance-based stability criterion for grid-connected inverters," *IEEE Trans. Power Electron.*, vol. 26, no. 11, pp. 3075–3078, Nov. 2011.

[24] X. Peng and H. Yang, "Impedance-based stability criterion for the stable evaluation of grid-connected inverter systems with distributed parameter lines," *CSEE J. Power Energy Syst.*, vol. 9, no. 1, pp. 145–157, Jan. 2023.

[25] C. Yoon, X. Wang, F. M. F. da Silva, C. L. Bak, and F. Blaabjerg, "Harmonic stability assessment for multi-paralleled, grid-connected inverters," in *Proc. Int. Power Electron. Appl. Conf. Exposit.*, 2014, pp. 1098–1103.

[26] W. Cao, S. Wang, K. Liu, H. Kang, and J. Zhao, "Responsibility identification for harmonic oscillation issues in the parallel grid-connected inverters system," *IEEE Access*, vol. 7, pp. 171061–171072, 2019.

[27] X. Wang, X. Ruan, S. Liu, and C. K. Tse, "Full feedforward of grid voltage for grid-connected inverter with LCL filter to suppress current distortion due to grid voltage harmonics," *IEEE Trans. Power Electron.*, vol. 25, no. 12, pp. 3119–3127, Dec. 2010.

[28] L. Zhou and Z. Mi, "Modeling and stability of large-scale PV plants due to grid impedance," in *Proc. 39th Annu. Conf. IEEE Ind. Electron. Soc. (IECON)*, Sep. 2013, pp. 1025–1030.

[29] D. Yang, X. Ruan, and H. Wu, "Impedance shaping of the grid-connected inverter with LCL filter to improve its adaptability to the weak grid condition," *IEEE Trans. Power Electron.*, vol. 29, no. 11, pp. 5795–5805, Nov. 2014.

[30] L. Jia, X. Ruan, W. Zhao, Z. Lin, and X. Wang, "An adaptive active damper for improving the stability of grid-connected inverters under weak grid," *IEEE Trans. Power Electron.*, vol. 33, no. 11, pp. 9561–9574, Nov. 2018.

[31] B. Shu, M. Gao, D. Zhang, K. Meng, R. N. Ashraf, and Y. Wang, "Control strategy of three-phase inverter under weak grid condition," in *Proc. Int. Conf. Smart Grids Energy Syst. (SGES)*, 2020, pp. 740–745.

CHENGBI ZENG received the B.S. and M.S. degrees in electrical engineering from Sichuan University, Chengdu, China, in 1987 and 1994, respectively, and the Ph.D. degree in circuit and system from the University of Electronic Science and Technology, Chengdu, in 2000. In 1994, she joined Sichuan University, as a Lecturer. She is currently a Professor with the College of Electrical Engineering, Sichuan University. Her research interests include microgrid, distributed generation, new energy power generation, and grid connection.

HONG MIAO received the B.S. degree in electrical engineering from the Hefei University of Technology, China, in 1992, the M.S. degree in power system engineering from Sichuan University, China, in 1995, and the Ph.D. degree in power electronics from Osaka University, Japan, in 2010. Since 1995, she has been with Sichuan University. Since 2010, she has been an Associate Professor with the College of Electrical Engineering, Sichuan University. Her research interests include application of power electronics, control of distributed generation and energy storage, technology of real time simulation, and power hardware-in-the-loop simulation.

XUEFENG WU received the B.S. degree from the Department of Power Engineering, North China Electric Power University (Baoding), Baoding, China, in 2019. He is currently pursuing the M.S. degree with the College of Electrical Engineering, Sichuan University, China. His research interests include the control scheme of grid-connected inverter, new energy power generation, and grid connection.
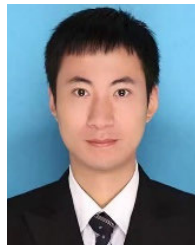
HAOXIANG DUAN received the B.S. degree in electrical engineering from the Chengdu University of Technology, China, in 2014, and the M.S. degree in electrical engineering from Sichuan University, China, in 2017. Since 2017, he has been an Engineer with Chengdu Rail Transit Group Company Ltd., China. His research interests include renewable energy generation and grid-connected technology.

• • •